Journal of Fluorescence (2019) 29:75–89
https://doi.org/10.1007/s10895-018-2312-6

ORIGINAL ARTICLE

A Fluorescent *Turn-On* Carbazole-Rhodanine Based Sensor for Detection of Ag^+ Ions and Application in Ag^+ Ions Imaging in Cancer Cells

Denzil Britto Christopher Leslee[1] · Sekar Karuppannan[1] · Muthu Vengaian Karmegam[1] · Sivaraman Gandhi[2] · Singaravadivel Subramanian[3]

Received: 30 August 2018 / Accepted: 14 October 2018 / Published online: 10 November 2018

Abstract

Carbazole – Rhodanine conjugate is an effective fluorescent host for silver ions through fluorometric transformation from green to red color with a hyperchromic emission. An intramolecular charge transfer process derived from carbazole towards rhodanine favors interaction of thiocarbonyl S and carboxylic acid O of the rhodanine moiety towards Ag^+ ion. Carbazole - rhodanine dyad accomplishes the lowest detection limit of 12.8×10^{-9} M and high quantum efficiency. A fluorescence reversibility of the probe with I^- ion surges reutilization of sensor molecule as an Ag^+ ion probe with minimal loss in the fluorescent efficiency. This fluorescent ligand is a biocompatible probe and is also a proficient candidate for fluorescent imaging of Ag^+ ion in live cells.

Keywords Fluorescent sensor · Silver ion · Carbazole · Rhodanine · Internal charge transfer · Cell imaging

Introduction

Silver an indispensable asset for human life, especially from the ancient times and was widely used as bactericidal and surgical prosthesis. In medicine, silver was cast as an antibacterial agent, used for treating mental illness and epilepsy [1]. It has potential application in the field of ornamentation, silverware and photographic industries and is used in dietary supplements. However, in contradict silver also impose large health impacts in the soluble as well as in the solid form of its existence [1–3]. Exposure to silver causes decreased blood pressure, diarrhoea, stomach irritation and decreased respiration, degeneration of fat in liver, kidney and causes argyrosis. Silver accumulates in skin, kidney, gingiva, mucous membranes, nails, cornea and spleen. Blood silver and urine excretion of silver are the indices for silver accumulation in human body [4, 5]. Also we know that silver has greater affinity towards thiols, in liver silver binds with reduced glutathione and depletes the amount of reduced glutathione available for the biochemical pathway and causes disorderliness of red blood corpuscles. Silver ion inactivates sulfhydryl enzyme and combines with amine, imidazole, and carboxyl groups of various metabolites [6–13]. The exploitation of silver nanoparticles for their commercial application has serious impact on respiratory system as damages the alveolar cell line, A549, dose dependent cellular toxicity, causes skin carcinoma and damages to DNA [14–16]. The admissible limits of silver recommended by the international health agency are, Permissible Exposure Limit (PEL) is 0.01 mg/m^3 (OSHA and MSHA), Recommended Exposure Limit (REL) 0.01 mg/m^3 (NIOSH), Threshold Limit Value (TLV) 0.1 mg/m^3 for metallic silver and 0.01 mg/m^3 for soluble silver (ACGIH, 1991), Time-Weighted Average (TWA) of 0.1 mg/m^3 (European Commission, 1994) [1, 17, 18]. Recently a huge concern has been raised among the researchers in liability for qualitative and quantitative estimation of the silver and silver component in environment and environmental suspects.

Although numerous sensors for the detection of silver have been developed, most of these are based on fluorescent quenching [19–25] and only a few have fluorescence enhancement [9, 26–32]. The fluorescent quenching response of certain sensor molecules for silver ion detection is due to

Electronic supplementary material The online version of this article (https://doi.org/10.1007/s10895-018-2312-6) contains supplementary material, which is available to authorized users.

✉ Sekar Karuppannan
karuppannansekar@gmail.com

[1] Department of Chemistry, Anna University – University College of Engineering, Dindigul 624622, India

[2] Institute for stem cell biology and regenerative medicine, Bangalore 560065, India

[3] Department of Chemistry, SSM Institute of Engineering and Technology, Dindigul 624002, India

the d^{10} configuration of silver which is known as fluorescence quencher via electron transfer, intersystem crossing (spin-orbit coupling process) and also due to the heavy metal ion effect [33–40]. In this paper a carbazole - rhodanine dyad receptor acts as a simple, selective, profound sensor for Ag^+ with an good application in cell imaging was developed [41]. We have opted for carbazole for because of its interesting behavior as a charge transfer ligand, hole transporting potential, electron donating nature and moreover, the carbazole derivatives are significant candidates in antimicrobial activity, dye sensitized solar cells, OLED, MOFs [42–48], and optochemical/electrochemical fluorescent sensor [49–58] which can be useful factors in fluorescence enhancement. The Rhodanine molecule linked to the signaling donor as a spacer unit (transducer), which has conjugative functionalized S, O, and N containing a pendant receptor serves as a good transducing and conjugative entity. Also, the Rhodanine molecules are renowned for their greater ability as a spectrophotometric reagent for determining heavy metals especially Ag, Au, Pd, and Cu [59–65]. Since carbazole and rhodanine systems have a longer excitation/emission wavelength and high fluorescence quantum efficiency this could be a most valuable feature for optical recognition of analytes. Hence, the strong electron delocalized structure of the probe, provides a remarkable spot-light for the silver ion, with a bathochromic shift in UV-Visible and hyperchromic shift in emission wavelength through Internal Charge transfer (ICT) mechanism. The bioimaging studies indicate that the probe could be a membrane permeable and a capable detector for Ag^+ ion in live cells. The probe harvests a fluorescent enhanced signaling with lowest limit of detection of range 10^{-9} M and high fluorescent quantum yield.

Experimental

Materials and Reagents

The materials used such as N-Ethyl Carbazole, Rhodanine 3-acetic acid, Acetic acid were purchased from Sigma Aldrich, India. Ammonium acetate, acetic anhydride, DCM, Phosphorous oxy chloride, DCE, Methanol and Hexane were procured from Central Drug House Ltd., India. Acetonitrile was bought from Merck, India and DMF was purchased from SRL, India. All metal nitrates were purchased from Merck, India. The solvents used for purification and optical analyses were distilled before usage.

Instrumentation and Measurements

The FT-IR analysis was performed in a Perkin Elmer Spectrometer using KBr pellet (Version 10.03.09), ^{1}H NMR spectra were recorded on a 300 MHz Bruker and the FT-NMR spectrometer in DMSO-d_6 with tetramethylsilane (TMS) as reference standard. The ^{13}C NMR spectra were recorded in 100 MHz frequency using Bruker FT-NMR spectrometer (400 MHz) in DMSO-d_6 with tetramethylsilane (TMS) as internal standard. Chemical shifts were reported in parts per million (ppm) and all coupling constant (J) are expressed in Hertz (Hz). The ESI-MS spectral analysis was performed in positive ion mode on a liquid chromatography-ion trap mass spectrometer (LCQ Fleet, Thermo Fisher Instruments Limited, US). The UV-Vis analysis was carried out by UV-Vis spectrophotometer (ANTECH, AN-UV-7000) with quartz cuvette of path length of 10 mm, silt width 1.0 nm and emission spectral studies are done using Spectrofluorometer (JASCO, FP 8200) with quartz cuvette of path length of 10 mm and silt width 5.0 nm. The surface topographical studies were done with a Vega3 Tescan model scanning electron microscope (SEM), The EDAX spectrum was recorded using Bruker Nano GMBH model. The fluorescence imaging was performed by Nikon confocal fluorescence microscope.

Synthetic Procedure

Synthesis of 9-Ethyl carbazolyl-3-carboxaldehyde (2)

The precursor 9-ethyl carbazolyl-3-carboxaldehyde **2** was synthesized by the procedure previously reported [66]. To DMF (3.74 g, 51.16 mmol) phosphorous oxychloride (7.85 g, 51.19 mmol) was added slowly with constant stirring for 30 min at 4 °C under a nitrogen atmosphere. 9-ethyl carbazole (**1**) (1 g, 5.12 mmol) in 10 ml of dichloroethane was added gradually to the above reaction mixture and refluxed at 90 °C for 10 h; the completion of the reaction was monitored by TLC with 100% Chloroform eluent. The product N-ethyl carbazole-3-carbaldehyde was extracted with chloroform, filtered and vacuum dried. This was further purified by column chromatography (silca gel; eluent $CHCl_3$-Hexane, 1:9) to obtain a pure yellow solid (**2**), 90% yield. ^{1}H NMR ($CDCl_3$, 300 MHz) δ_H (ppm): 10.06 (1H, s), 8.57 (1H, s), 8.12 (1H, d, J = 8.4 Hz), 7.97 (1H, d, J = 8.4 Hz), 7.51 (1H, t, J = 8.4 Hz), 7.43 (2H, m, 8.1 Hz), 7.30 (1H, t, J = 8.1 Hz), 4.31 (3H, q, J = 7.2 Hz), 1.43 (2H, t, J = 7.2 Hz). Mass (ESI-MS): 224.1081 m/z.

Synthesis of 2-(5-(9-Ethyl carbazol-3-yl)methylene) -4-oxo-2-thioxothiazolidin-3-yl)acetic acid (CR-3)

To a solution of 9-Ethyl carbazole-3-carboxaldehyde (**2**) (0.5 g, 2.24 mmol) in 25 ml of acetic acid, rhodanine-3-acetic acid (0.85 g, 4.40 mmol), ammonium acetate (0.39 g, 5.00 mmol) followed by acetic anhydride (0.411 g, 4.00 mmol) were added. Then the mixture was stirred at 100 °C for about 8 h. The formed residue was allowed to cool at room temperature, filtered, washed three times with distilled water and

dried. The crude residue was purified by column chromatography using the eluent DCM/MeOH (4:1) on silca gel to afford a pure brick red solid with 95% yield [9, 41, 67]. ^{1}H NMR (DMSO-d_6, 300 MHz), δ_H (ppm): 8.50 (1H, s); 8.30 (1H, d, J = 9 Hz); 8.05 (1H, s); 7.77 (2H, m);7.54 (2H, t, 9 Hz); 7.30 (2H, t, 9 Hz); 4.72 (2H, s); 4.50 (2H, m); 1.34 (3H, t). ^{13}C NMR (DMSO-d_6, 100 MHz), δ_C (ppm): 193.62, 167.87, 166.97, 141.46, 140.72, 136.15, 129.12, 127.33, 124.94, 124.10, 123.56, 122.44, 121.42, 120.54, 117.74, 110.85, 110.34, 45.73, 37.93, 14.24. FTIR (KBr, cm^{-1}): 3121, 3050, 2979.32, 2934.98, 1749.55, 1670.27, 1570.21, 1494.17, 1407.29, 1336.38, 1236.91, 1192.94, 1156.68, 1116.80, 1060.16, 806.56, 742.42, 606.81, 561.68, 515.59, 478.88, 439.16, 421.02. Mass (ESI-MS): 396.0698 m/z.

Preparation of Solution Samples for Photophysical Studies

The Stock solutions of metal ion (Zn^{2+}, Pb^{2+}, Ni^{2+}, Na^{2+}, Mn^{2+}, Mg^{2+}, K^{+}, Hg^{2+}, Fe^{2+}, Fe^{3+}, Cu^{2+}, Co^{2+}, Cd^{2+}, Ca^{2+}, Ba^{2+}, Al^{3+} and Ag^{+}) and anions (CH_3COO^{-}, CO_3^{2-}, HSO_4^{-}, I^{-}, F^{-}, Cl^{-}, Br^{-}, SCN^{-}, CN^{-}, $H_2PO_4^{-}$ and S^{2-}) were prepared to 1 mM in HEPES buffer (20 μM, pH 7.5). A stock solution of **CR-3** (1 mM) was prepared with CH_3CN, and these stock solution of 1 mM metal ion, anions and probe **CR-3** were diluted to 10 μM by proper dilution with CH_3CN/H_2O (1:9) buffer (pH 7.5, 20 μM HEPES). The metal salts utilized in the studies were taken as nitrate salt, in account of reducing the interference of the counter ion. All optical studies were performed in CH_3CN/H_2O (1:9 *v*/v, 20 μM HEPES buffer, pH 7.5) at room temperature and other analytical conditions.

HeLa Cell Culture

The HeLa Cells were cultured as a monolayer in Eagle's minimal essential medium (EMEM) at 37 °C, humidified atmosphere in air; culture medium was nurtured with 10% FBS (Foetal Bovine Serum). After incubation, the remaining supernatant medium containing dead cells was aspirated, and then the culture containing live cells was washed with 2 × 10 ml aliquots of Phosphate Buffered Saline solution to remove excess serum. HeLa cells were again dispersed in the medium for incubation in 3 ml trypsin-PBS solution (0.25% trypsin) for 5 min at 37 °C. This was followed by the addition of 10% FBS (5 ml) containing EMEM to inactivate the trypsin. The solution was then centrifuged for 5 min to remove any remaining dead cells; the resulting supernatant liquid was sucked off and cell medium were transferred to the remaining cell lines.

MTT Assay Procedure

MTT assay was performed to assess the cyctotoxic effect of probe **CR-3** on the HeLa cell lines. In the dose dependent MTT assay, the cell lines were first done with control experiments prior to incubation of **CR-3** for live cell imaging. After this, each aliquot of HeLa cells lines were treated with different dose concentrations of **CR-3** probe say, 0.01 μM, 0.1 μM, 0.5 μM, 1 μM, 5 μM, 10 μM, and 20 μM in 1% DMSO, 99% serum free EMEM and incubated at 37 °C for 1 h. The cell lines were washed three times with PBS solution to remove remaining **CR-3** probe and dead cells. This was followed by the addition of 10 μL MTT solution and the assay medium was further incubated for 1 h at 37 °C in dark. Thereafter the medium was washed with PBS and added with 100 μL DMSO to dissolve the formed formazan crystals. The solution medium was triturated homogeneously and the absorbance was recorded at 570 nm using ELISA plate reader.

The time lapse assay was carried out in a similar method to that described above but with appropriate concentration of probe **CR-3** say 10 μM in 1% DMSO, 99% serum free EMEM incubated at 37 °C in dark for different time lapse such that 1, 3, 6, 9, 12, 15, 18 and 24 h of incubation period. After each incubatory period, each plate well was processed with 10 μL MTT as performed in the dose dependent assay and the absorbance were recorded at 570 nm.

For determination of half minimal metabolism inhibitory value (Ic_{50}) by application of MTT assay, the HeLa cell lines were incubated with varied concentrations of **CR-3** solution such as 1 μM, 10 μM, 50 μM, 100 μM, and 250 μM (in 1% DMSO, 99% EMEM containing 10% FBS) at 37 °C for 48 h. After the period of incubation the cells were washed with 3 × 10 μL (10%) PBS solution, followed by incubation for 1 h with 100 μL of MTT solution (MTT 0.5 mg/mL and a 10% mixture of PBS and serum free medium). The resulting supernatant liquid was aspirated, the medium was then dissolve with 100 μL DMSO and the absorbance were recorded on ELISA plate reader.

Fluorescence Cell Imaging

For fluorescence imaging of Ag^{+} ion in HeLa cells, the **CR-3** probe was tested for effectiveness of its non-cyctotoxic nature on HeLa cell lines using MTT assay method. Prior to incubation with **CR-3**, the cells were washed with PBS solution to remove any dead cell matters. The HeLa cell lines were then added with **CR-3** (in aqueous DMSO, serum free medium) to obtain a final concentration of 10 μM **CR-3** in 1% DMSO; incubated at 37 °C for 30 min in dark. After the incubation, the cell lines were washed with PBS to remove excess **CR-3** samples, dead cells, and the supernatant medium was sucked off and fresh serum free medium (SFM) was added, immediately the confocal images were recorded at $\lambda_{ex}/\lambda_{em}$ = 442 nm/460–650 nm. The above **CR-3** treated cell lines were washed three times with PBS. The supernatant liquor was aspirated and added with serum free medium (SFM). Thereafter, the cell lines were incubated with Ag^{+} ion solution (to final

concentration of 10 μM Ag^+ in aqueous medium) for 10 min at 37 °C. The cell medium was then washed with PBS buffer and then cells were observed using confocal Fluorescence microscopy at $\lambda_{ex}/\lambda_{em}$ = 442 nm/460–650 nm.

Results and Discussion

Synthesis

9-Ethyl carbazolyl-3-carbaldehyde (2)

The precursor 9-ethyl carbazolyl-3-carbaldehyde (**2**) was successfully synthesized by Vilsmeier – Hack formylation of 9-Ethyl carbazole (**1**) with $POCl_3$ and DMF in DCE. *9-ethylcarbazolyl-3-carbaldehyde* (**2**), a yellow solid, 90% yield. The product was characterized and confirmed by ^1H NMR and ESI- Mass spectrometry. (See supporting information).

2-(5-((9-Ethyl carbazol-3-yl)methylene) -4-oxo-2-thioxothiazolidin-3-yl)acetic acid (CR-3)

The probe **CR-3** was synthesized by treating 9-Ethyl carbazolyl-3-carbaldehyde (**2**) with rhodanine-3-acetic acid in presence of ammonium acetate and acetic anhydride in acetic acid as shown in Scheme 1. *2-(5-((9-Ethyl-carbazol-3-yl)methylene)-4-oxo-2-thioxothiazolidin-3-yl)acetic acid* (**CR-3**), a brick red powder, 95% yield. The probe **CR-3** was characterized by NMR, FTIR and ESI- Mass spectroscopy. (See supporting information).

Optical Analysis of Probe CR-3 Sensing Ag^+ Ion

The selectivity of **CR-3** probe for Ag^+ ion was established by photophysical studies of the probe with various metal ions and the sensitivity of the probe **CR-3** was also monitored by titration analysis. The absorbance spectra for the probe **CR-3** (10 μM) was done with various competitive metal ions say, Zn^{2+}, Pb^{2+}, Ni^{2+}, Na^{2+}, Mn^{2+}, Mg^{2+}, K^+, Hg^{2+}, Fe^{2+}, Fe^{3+}, Cu^{2+}, Co^{2+}, Cd^{2+}, Ca^{2+}, Ba^{2+}, Al^{3+} and Ag^+ ions (10 μM) in CH_3CN/H_2O (1:9) buffer (pH 7.5, 20 μM HEPES) (Fig. 1a).

The UV-Vis spectrum of the free probe **CR-3** showing two absorption bands at 289 nm and 442 nm, where the weak absorption peak at 289 nm corresponds to π-π* transition of the conjugated system and the strong band over 442 nm was assigned to the ICT process between carbazole unit and the rhodanine-3-acetic acid of the probe with efficient charge separation. Consequently, on the addition of 10 μM Ag(I) solution, the probe shows a strong ICT enhanced red shift from 442 nm to 466 nm whilst the other competing ions have no significant remarks on the absorbance of the probe. Also, the change in absorbance of the probe towards variable equivalence of silver ion was studied in acquiring the binding nature of the **CR-3** with Ag^+ ion. A gradual drop in the intensity to extent of about 500 nm and thenceforth a raise in height were notified, this shows a 1:1 binding nature was thus involved (Fig. 1b). Thus a charge transfer electron delocalization takes place from carbazole to the sulphur and oxygen atom of rhodanine moiety led to large electron density favouring a possible ground state formation. These results state that an intramolecular charge transfer (ICT) mechanism was involved in **CR-3** detection of Ag^+ ion.

The emission spectra of sensor **CR-3** (10 μM) with distinguished metal ions (10 μM) in CH_3CN/H_2O (1:9) mixture buffered with 20 μM HEPES (pH 7.5) has been performed. The Fig. S5, shows intramolecular charge transfer enhanced red shift in emission at 548 nm of the probe **CR-3** in the Free State with excitation at 442 nm absorbance, while on exposure of silver ion (10 μM) the emission profile shows a specific enhancement in the emission intensity around 548 nm for silver ion; additionally, almost all the other interfering metal ions has no apparent variation in the fluorescence emission of **CR-3**. Similarly, the fluorescence titration was carried out with different concentration of silver ions (Fig. 2), and shows a subsequent gradual increase in fluorescence intensity with increase in equivalence of Ag^+ ions solution, providing an fluorescence turn-ON behavior by formation of an strong ICT process for selective detection of Ag^+ ion.

The probe also could be a colorimetric sensor for silver ion in visible light to approximate limit of 10^{-4} M range. The Fig. 3 shows the photo images of fluorescent and colorimetric detection of silver ion in UV-lamp and visible light respectively at increasing concentration levels at

Scheme 1 Synthesis of probe CR-3

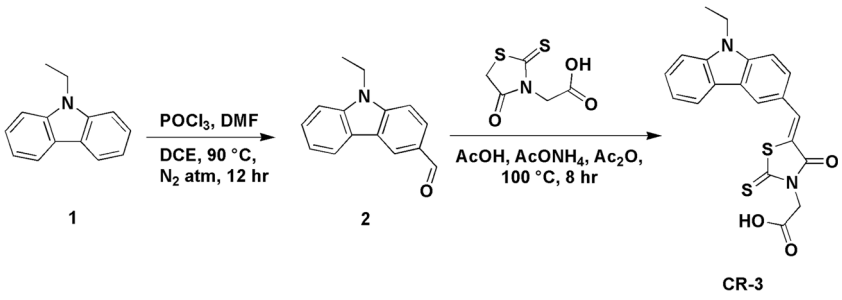

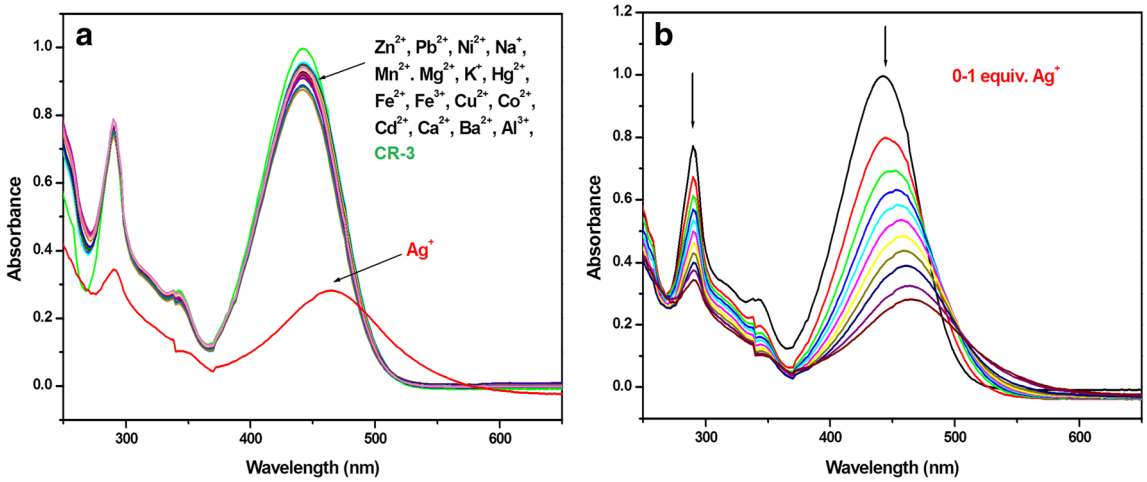

Fig. 1 Absorption spectra of (**a**) **CR-3** with different metal ions in CH_3CN/H_2O (1:9) buffer (pH 7.5, 20 μM, (**b**) **CR-3** with an increasing concentration of Ag^+ ions in CH_3CN/H_2O (1:9) buffer (pH 7.5, 20 μM HEPES)

10^{-4} M, with increasing color change from fluorescent green to fluorescent red in UV-light and yellow to red in visible light, which reveals the possibility of naked eye detection of silver ions.

By using Fluorescein ($\Phi_{ref} = 0.95$) in aqueous NaOH at room temperature, as a standard fluorescence reference, the relative fluorescence quantum yields at $\lambda_{ex}/\lambda_{em} = 442$ nm/548 nm was calculated using the formula shown in Calculation 1.1. (See supporting information). The relative quantum yield of the free probe **CR-3** ($\Phi_{CR\text{-}3}$) was found to be 0.06 and while on addition of 1 equiv. Ag^+ ion to **CR-3**, the fluorescence intensity increases with a quantum yield of metal complex CR-3 + Ag^+ ($\Phi_{CR\text{-}3+Ag}$) reaches to 0.53, which indicates a high fluorescence quantum efficiency yield of **CR-3** for Ag^+ ion.

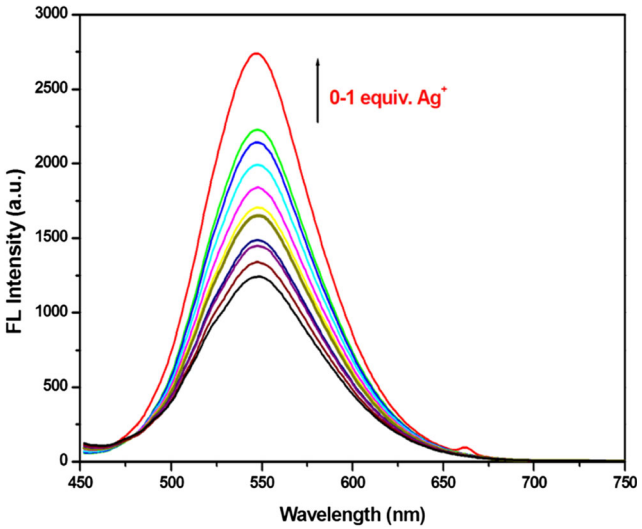

Fig. 2 Emission spectrum of **CR-3** titrated with 0–1 equiv. of 10 μM Ag^+ solutions in CH_3CN/H_2O (1:9) buffer (pH 7.5, 20 μM HEPES)

Influence of Physicochemical Factors and Conditions on Fluorescence Response of CR-3 with Ag^+ Ion

Interference of Co-Existing Ions

A Bar diagram was plotted for the fluorescence response of the probe **CR-3** with varied metal ion added with Ag^+ ion solution maintained at pH 7.5 at λ_{em} 548 nm. The plot shown in Fig. 4 reveals the sensitivity and selectivity towards the silver (I) ion in competing with the other interfering ions. The blue bar corresponds to the fluorescence probe **CR-3** with Ag^+ ion in presence of other metal ions, that renders a very minimal percentage fluorescence quenching to about ~2% in coexistence with other metal ions. This evidence reveals the sensitivity and selectivity of probe with very finite grade of emission variation and good stability of the **CR-3** + Ag^+ complex in co-existence with interfering metal ions.

Effect of pH

The influence of pH on fluorescence response of **CR-3** to Ag^+ detection was done at $\lambda_{em} = 548$ nm at varying pH values ranging from 1 to 14 at room temperature regulated with HEPES buffer solution. The Fig. 5a replicate that at an acidic pH (0 to 5) the fluorescence of the both **CR-3** and **CR-3** + Ag^+ complex was quenched, this might be due to the partial protonation of the thiocarbonyl sulfur atom, that inturn restrict the interaction of Ag^+ ion with sulfur. While around a pH value of 6.0–9.0, the fluorescence was enhanced to the higher quotient with stable and steady emission profile.

On increasing the pH to 9.0 the fluorescence intensity slightly get reduces and on further increasing the pH of the solution, the intensity drops down gradually this might be pertain to the formation of AgOH or the partial base hydrolysis of carboxylic acid group. From this observation it is

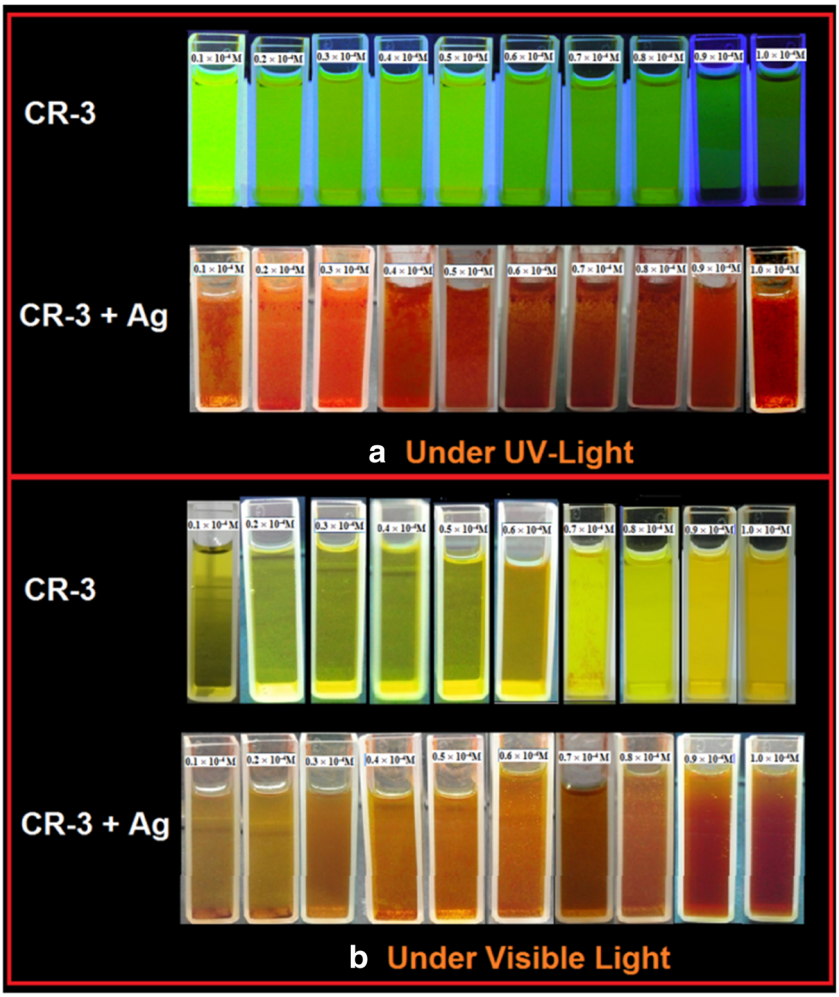

Fig. 3 Photography of Fluorescent and Colorimetric Images of **CR-3** and **CR-3** + Ag^{+} complex

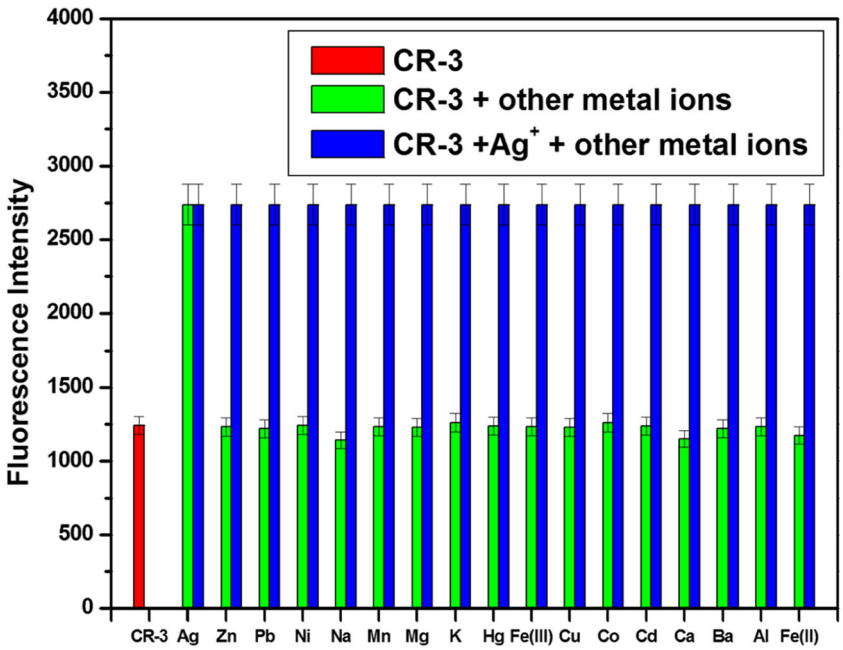

Fig. 4 Fluorescence response of **CR-3** with Ag^{+} ion in co-existence of other metal ions at $\lambda_{em} = 548$ nm

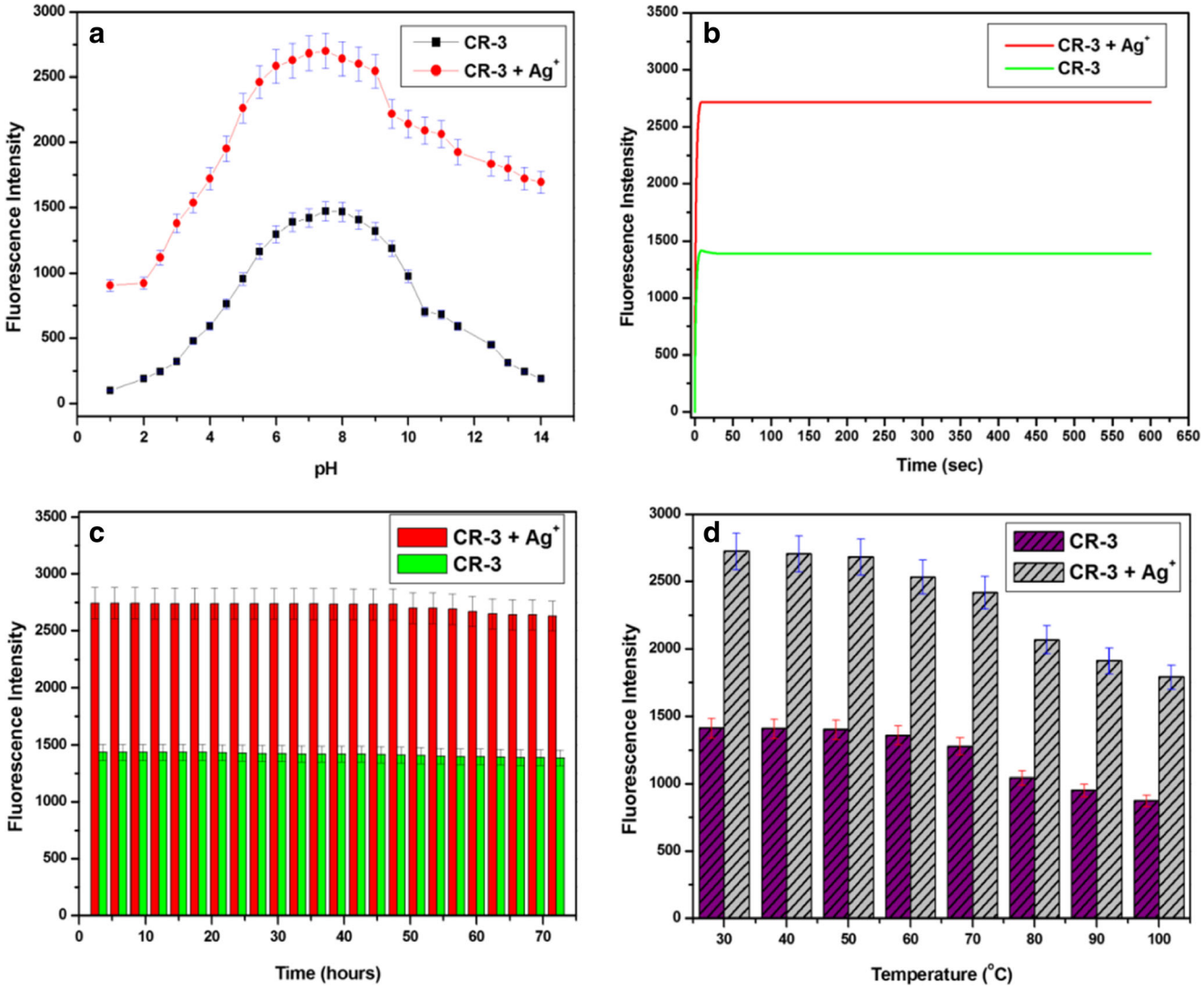

Fig. 5 **a** Fluorescence response **CR-3** and **CR-3** + Ag^+ complex to variable pH range at $\lambda_{em} = 548$ nm. **b** Fluorescence response time **CR-3** with Ag^+ at $\lambda_{em} = 548$ nm in CH_3CN/H_2O (1:9) buffer (pH 7.5, 20 μM HEPES). **c** Standing time fluorescence of **CR-3** and **CR-3** + Ag^+ at 548 nm in CH_3CN/H_2O (1:9) buffer (pH 7.5, 20 μM HEPES). **d** Temperature dependent fluorescence response of **CR-3** and **CR-3** + Ag^+ at 7.5 pH 20 μM HEPES buffer (CH_3CN: H_2O, 1:9) at $\lambda_{em} = 548$ nm

evident that the pH range around 6 to 9 is favorable for **CR-3** and Ag^+ ion bounding with enhanced fluorescent emission. Hence a pH of 7.5 was chosen as the optimum condition for the photophysical and physiological studies, since the neutral pH range is a more acceptable medium for the cell imaging in biological application.

Response Time and Standing Time Fluorescence

For real time applications, the fluorescence response of **CR-3** and **CR-3** + Ag^+ complex was correlated with a time course fluorescence experiment at an emission wavelength of 548 nm in room temperature, the time dependent plot (Fig. 5b), shows that **CR-3** fetch a very rapid response to Ag^+ ions a time of less than 2 s in forming **CR-3** + Ag^+ complex with sharp hyperchromic shift in fluorescence intensity.

Subsequently, the standing time fluorescence analysis was performed for the time dependent influence on the fluorescence of the probe and the complex at room temperature. From the Fig. 5c, it can be noticed that a steady emission for about 24 h and thereafter a stable fluorescence with minimum deviation for about a period of 48 h was noted. From these studies, it was clear that the probe could provide a spontaneous response to the silver (I) ion which is a potential gradient for application of **CR-3** sensor in environment and biological systems with a quiet stable fluorescence emission over 48 h of standing at room temperature.

Effect of Temperature

A temperature dependent fluorescence assay of the probe **CR-3** and the **CR-3** + Ag^+ complex in CH_3CN: H_2O (*v*/v, 1:9)

buffer (20 μM HEPES, pH 7.5) was carried out from 30 °C to 100 °C temperature at λ_{em} 548 nm. The bar diagram representation in Fig. 5d demonstrates the violet bar, which describes the fluorescence of **CR-3** and the ash colored bar for the fluorescence response of **CR-3** + Ag^+ complex on effect of increasing temperature.

From the Fig. 5d, it was noticed that to about 70 °C the fluorescence of the probe as well as the complex was relevantly stable and besides the 70 °C the fluorescence of the **CR-3** + Ag^+ complex and **CR-3** was filtered downward, this might be due to the distortion or larger polarization of the bonds between S, O of rhodanine moiety and Ag^+ ion.

Effect of Counter Ion

The sensor complex **CR-3** + Ag^+ was also tested for the fluorescent reversibility with various counter anions like CH_3COO^-, CO_3^{2-}, HSO_4^-, I^-, F^-, Cl^-, Br^-, SCN^-, CN^-, $H_2PO_4^-$ and S^{2-}. From the Fig. 6a & b, it can be culminated that 1 equivalent addition of I^- brought about an appreciable restoration in fluorescence of **CR-3** probe in CR-3 + Ag^+ ensemble, while all other anions showed least variation in fluorescence.

The effect of I^- ion on the complex (**CR-3** + Ag^+) intensity was almost reached that of the free probe CR-3, as since it is well known that I^- bind strongly to Ag^+ ion and possibly forms AgI in solution. Thus it proves that the fluorescence of **CR-3** with Ag^+ ion can be reversible in presence of I^- ions. A cyclic reversibility assay was conducted with **CR-3** towards cyclic addition of Ag^+ and I^- in countering way (Fig. 7), this shows a fluorescence enhancement with Ag^+ and relaxation with next cycle of I^- ion; and this pattern was continued to five cycles of alternative addition of Ag^+ and I^- ions with a little loss of fluorescent efficiency at each cycle. Hence, it is firm that the probe **CR-3** could be considered as "dual" fluorescent probe.

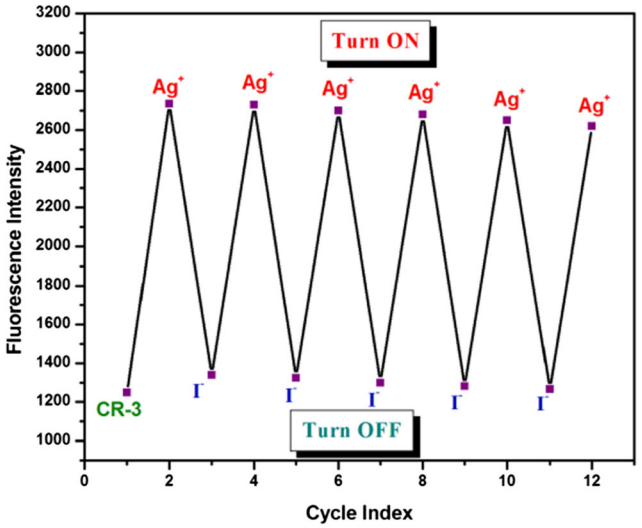

Fig. 7 Emission Reversibility Cycle of **CR-3** with cyclic addition of Ag^+ and I^- ion at λ_{em} = 548 nm in CH_3CN:H_2O (1:9), (7.5 pH, 20 μM HEPES buffered)

Binding Mode Analysis

Binding Properties

To confirm the stoichiometry of the binding of probe **CR-3** with Ag^+ ion the Job's plots analysis was carried out. By a continuous variation method of absorbance and fluorescence spectra, the Job's plots were obtained from the absorbance variation at 466 nm against mole fraction of Ag^+ ion and plot of fluorescence difference at 548 nm to mole fraction of Ag^+ ion clearly showed the maxima at mole fraction of 0.5 indicate that the formed complex was a 1:1 stoichiometric ensemble (Fig. S7).

The binding constant of **CR-3** with Ag^+ was calculated from the fluorescence titration spectra using the formula shown in **Calculation 1.3.** (See supporting information) and

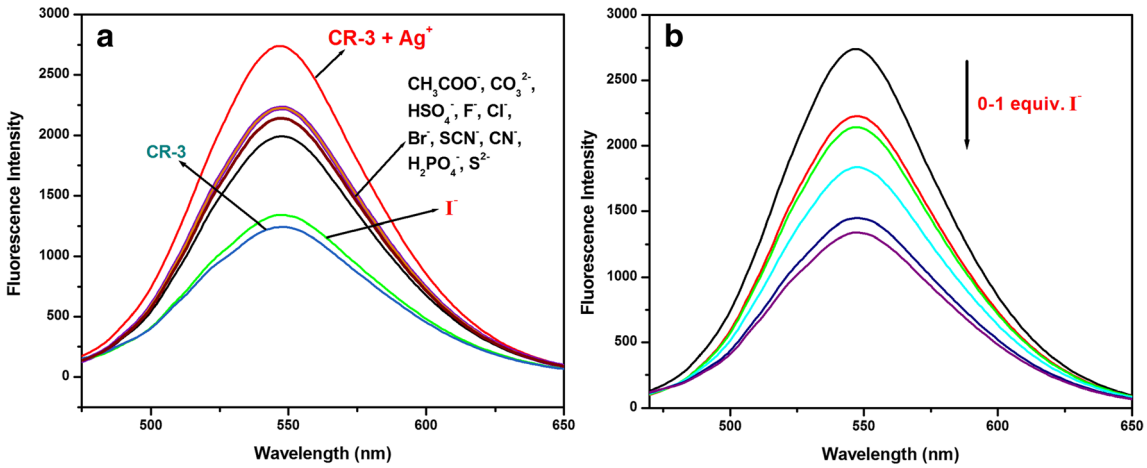

Fig. 6 Fluorescence Reversibility Assay of **CR-3** + Ag^+ complex in HEPES buffer (at 7.5 pH, CH_3CN: H_2O (1:9)) (**a**) with addition of distinct counter anion, (**b**) with increasing concentration of I^- ion

K_a value was found to be 3.8×10^4 M^{-1} [68]. A linear response of the fluorescence intensity as a function of [Ag^+] was observed from 30 nM to 1 μM ($R^2 = 0.9985$) shown in Fig. S8 (See supporting information). From the slope of the linear fit (Fig. S8), the Limit of Detection (LOD) of the probe **CR-3** for Ag^+ ion was determined using the formula shown in **Calculation 1.4.** (See supporting information) and was found to be 12.8×10^{-9} M [69]. The finding of photophysical parameters were summarised in the following table (Table 1).

A comparison on detection limits of the present work with formerly reported fluorescent probes was carried out as shown in Table S1 (See supporting information). The Table S1 reveals that the probe **CR-3** might be a good sensor for silver (I) ion with fluorescent enhancement and a lowest detection limits in 90% of water solubility with HEPES buffered.

Sensing Mechanism

In order to understand the binding nature and plausible interaction of the probe **CR-3** and Ag^+ ion the following analytical studies were conducted.

The ^{1}HNMR was performed for free probe **CR-3** and **CR-3** after addition of 1 equiv. Ag^+ ion in DMSO-d_6 solvent. From the Fig. 8, it was noticed that the complex peaks of **CR-3 + Ag$^+$** are doesn't seem to be as sharp as the free probe peaks and almost all the peaks are slightly deviate in chemical shift from that of the free probe.

However, the proton (H_e) peak of O-H group at 8.50 ppm of free probe **CR-3** shifts downfield to 8.77 ppm on complexation with Ag^+ ion, this might be due to the binding of the oxygen atom of hydroxyl group to Ag^+ ion. Hence, the intramolecular electron potential experienced by the rhodanine moiety, might cause disturbance in the electronic spin character of the hydroxyl oxygen atom and the possible spatial electronic delocalisation due to the anisotropic moment over [–C=S] group might also be the reason for downfield shift of hydroxyl proton.

The FTIR analysis of the free probe **CR-3** and **CR-3** with Ag^+ were performed, and spectrum is shown in the Fig. 9. The Fig. 9 shows a characteristic change in the O-H stretching region of the carboxylic acid group, as bands at 3121.10 cm^{-1} and 3050.90 cm^{-1} get disappeared for **CR-3 + Ag$^+$** complex and a new stretching bands at 3407 cm^{-1}, 3214.19 cm^{-1} was appeared for 1:1 composition. Consecutively, the O-H bending vibration of the probe **CR-3** vanished at 1441.49 cm^{-1} on complexation.

Due to the highly conjugated electron charge resonating system of the probe and also the strong affinity nature of silver towards sulphur, the silver ion get attracted to S atom (-C=S). Thus, when the silver ion approaches the thiocarbonyl group, the sulphur atom suffers charge deficiency; this charge deficiency was simultaneously stabilized by the delocalization of electronic charge by ICT process, hence the thiocarbonyl sulphur atom forms a strong bond with silver. In addition, owing to ICT process and the anisotropic moment over [-C=S] group have imposed a partial charge separation of –O-H group and this charge separation inturn leads to the interaction of oxygen atom (–O-H group) with silver ion.

While due to the ICT process, the rhodanine N atom is not involved in the interaction with silver ion, this because since a higher affinity of Ag^+ ion binding to sulphur atom [S=C-N] unit and the larger electronegativity of oxygen atom (-COOH) reduces the electron density on N atom. Also, the existence of the methylene ($-CH_2$) group further reduces the acidity of the amide nitrogen of the ring, this makes the ring nitrogen atom less available for coordination [&, 59, 60, 63, 64, 70–74]. As a result an intense band for $[C\text{-}N]_{str}$ at 1391.20 cm^{-1}, and a comparative reduction in peak intensity of the $[C=S]_{str}$ with a slight shift from 1336.38 cm^{-1} (C=S) was noticed. In addition, due to the most stable ICT resonating system, the band at 1192.94 cm^{-1}, 1156.68 cm^{-1}, and 1116.80 cm^{-1} of [-C=S] stretching get slightly shifted and decreased in height on complexation.

Further, the mass spectrum of the complex shows a predominant 1:1 complex peak at 501.9612 m/z and also establishes a minor peak at 899.1286 m/z which express the minimal opportunity for formation of 2:1 stoichiometry. Thus in compliment to the other spectral evidence, the mass spectra also enumerate the formed **CR-3-Ag** complex is a 1:1 binding proportionate sensor (Figs. S4 and S6). (See supporting information). Thus with the countenance of above analytical evidence, we proposed a 1:1 binding mode mechanism of the probe **CR-3** with Ag^+ ion shown in Scheme 2.

DFT Analysis

The geometries of the probe **CR-3** and the complex **CR-3 + Ag$^+$** were optimized using DFT calculations by a Gaussian 09 program with B3LYP and 6-311G/LANL2DZ basis sets [75]. From the optimized geometries the π electrons distribution and orbital energies of HOMO and LUMO of **CR-3** and [**CR-3-Ag**] were also determined (Fig. 10). The HOMO-

Table 1 Measured and calculated parameters of **CR-3** and **CR-3 + Ag$^+$** complex

λ_{ex} (nm)	λ_{em} (nm)	Association Constant (M^{-1})	Detection Limit (M)	Quantum Yield (Φ)	
				CR-3 ($\Phi_{CR\text{-}3}$)	**CR-3 + Ag$^+$** ($\Phi_{CR\text{-}3+Ag}$)
442	548	3.8×10^4	12.8×10^{-9}	0.06	0.53

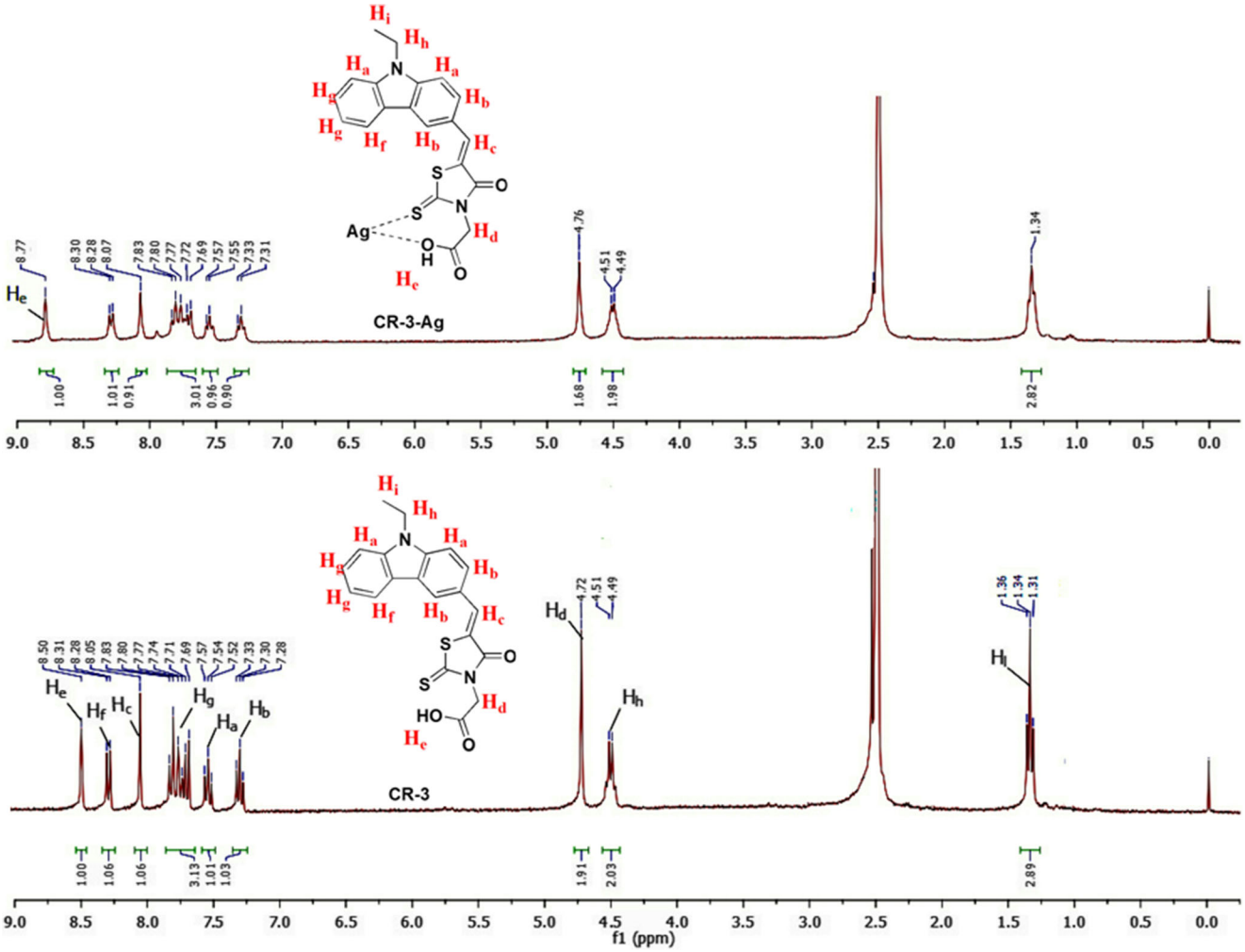

Fig. 8 ^{1}HNMR (300 MHz) titration spectrum of **CR-3** and **CR-3-Ag**$^{+}$ in DMSO-d_6

LUMO excitation of FMO's of **CR-3** and **CR-3** + **Ag**$^{+}$ complex moves the electron crowd from the carbazole to rhodanine-3-acetic acid unit through the intramolecular charge transfer process. From the Fig. 10, it is visible that the FMOs at excitation the π electrons cloud on the HOMO of **CR-3** is highly positioned on the carbazole moiety and slightly on the rhodanine moiety where the LUMO of **CR-3** mostly mounted on the rhodanine and slightly over the carbazole unit that intimating the ICT process involved in the excitation level. Whereas, in the excited state FMOs of **CR-3** + **Ag**$^{+}$ complex

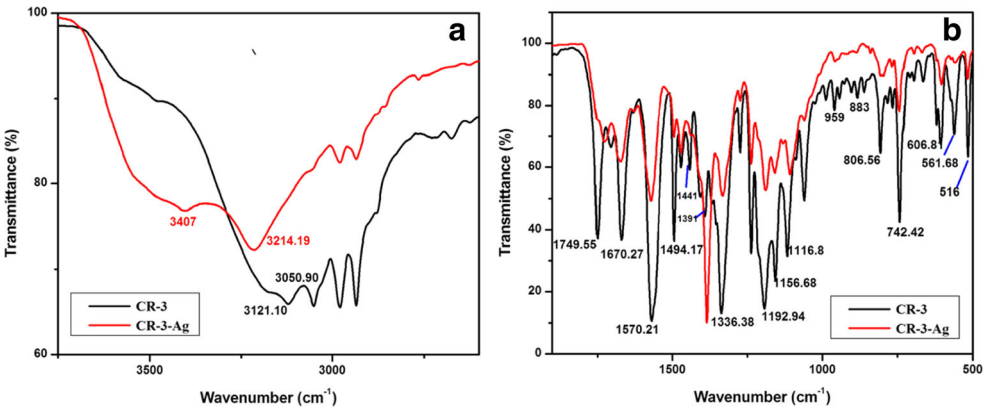

Fig. 9 Partial FTIR spectrum of **CR-3** and **CR-3-Ag**$^{+}$: **a** comparative FTIR spectrum from 3750 to 2600 cm^{-1}, **b** comparative FTIR spectrum from 1800 to 500 cm^{-1}

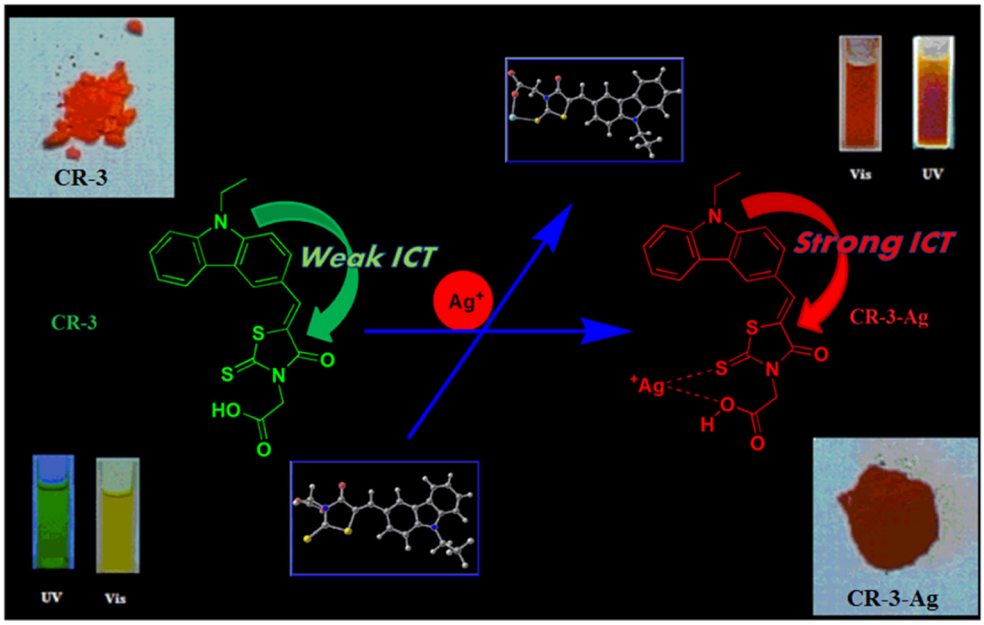

Scheme 2 Proposed sensing mechanism of probe **CR-3** towards Ag^+ ion

the π electrons density on HOMO is mainly located on the whole π-conjugated rhodanine framework, the LUMO largely positioned at the center of the guest Ag^+ ion, this confirms strong ICT process that took place on interaction of **CR-3** probe with Ag^+ ion.

Moreover, the HOMO–LUMO energy gap of the complex becomes much smaller relative to that of probe **CR-3**, hence the energy gaps between HOMO and LUMO in the probe **CR-3** and [**CR-3-Ag**] complex was found to be 3.17 eV and 2.77 eV respectively. The optimized geometries shown in the Fig. S9 clearly exposes that the Ag^+ ion binds through two coordination sites of the probe. Hence, the interaction of the Rhodanine S atom (thiocarbonyl sulphur, [-C=S]) and O atom (hydroxyl oxygen atom, [-COOH]) with Ag^+ reflects on the FMOs and accompanied change in the orbital energy level, revealing the optical detection.

Morphological and Elemental Analysis

The Scanning Electron Microscopic (SEM) images of **CR-3** and **CR-3** + Ag^+ differ dramatically in surface topography as shown in Fig. 11. The probe **CR-3** shows a random needle like structural projection in Free State, whilst the complex **CR-3-Ag**$^+$ exhibits a closely packed and spherically crowded

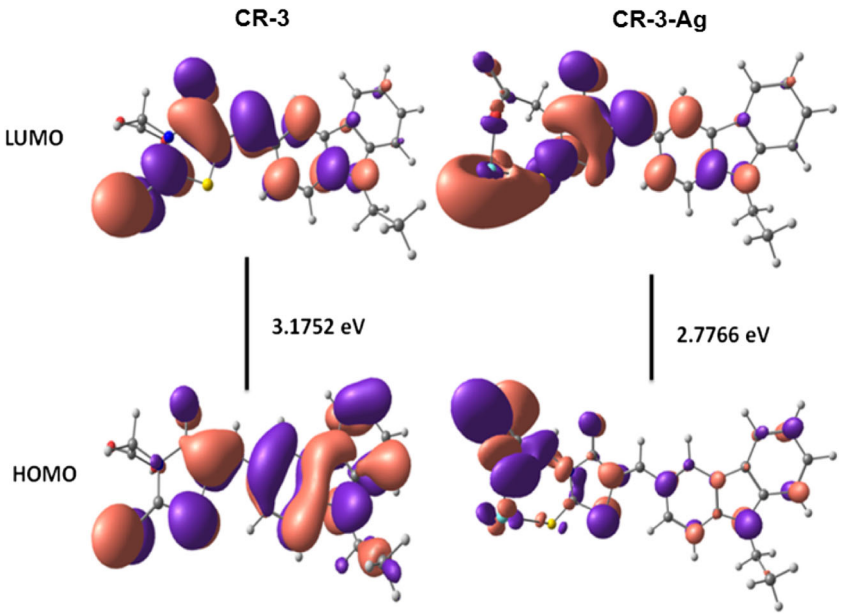

Fig. 10 Calculated (B3LYP/6-31G*) structure for **CR-3** and **CR-3** + Ag^+ complex

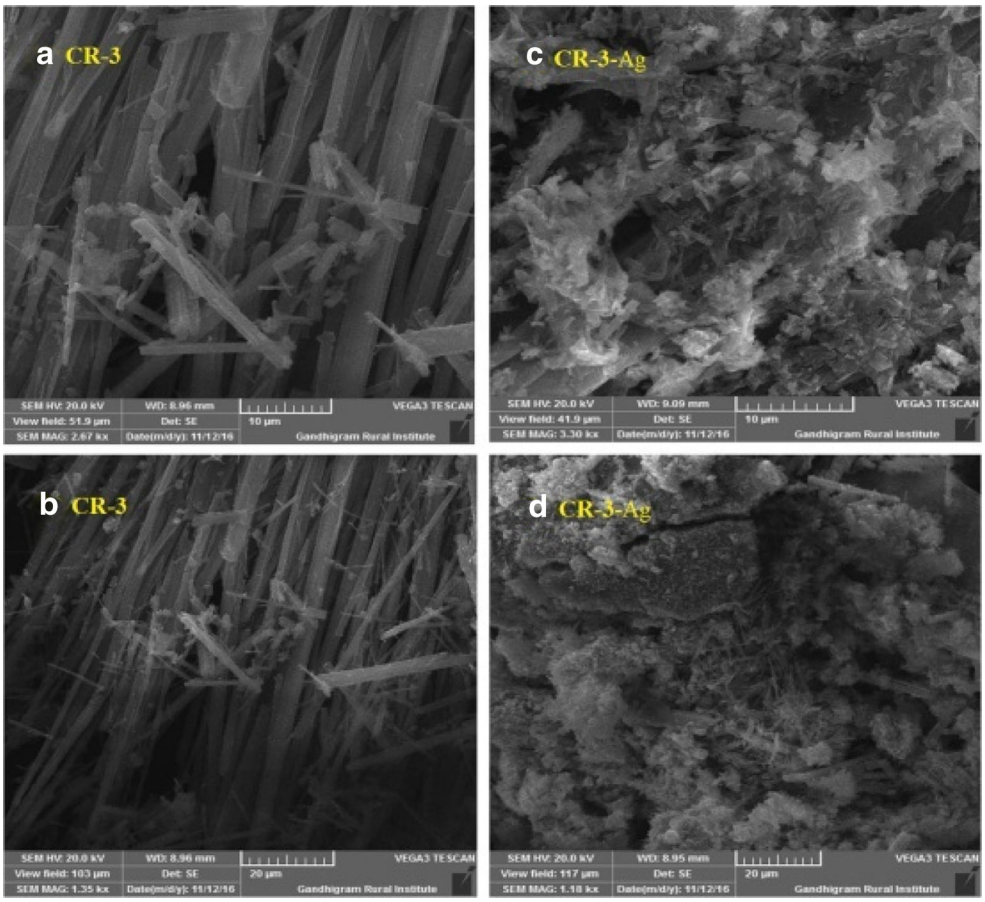

Fig. 11 SEM images of **CR-3** and complex **CR-3-Ag**; **a** at 10 μm **b** at 20 μm

structures. This spherical morphological change is due the formation of a self assembling that exposed between the **CR-3** and Ag^+ ion. The steric hindrance effect of the bulkier carbazole unit and carbon-carbon single bond rotation of carbazole and rhodanine acetic acid groups pushed the acid end and sulphur to twist out of the plane of the **CR-3** probe, which restrict the formation of stacking model but rather forms a 1:1 **CR-3-Ag**$^+$ complex, which was also ascertained by the optimized geometries of probe and metal complex represented in Fig. S9 [76].

The chemical composition of the probe **CR-3** and the complex **CR-3-Ag**$^+$ was enumerated from EDX analysis (Fig. S10), which clearly indicates the presence of the carbon (C), oxygen (O), nitrogen (N) and sulphur (S) in the free probe **CR-3**; while in the complex form along with other element the presence of silver (Ag) shows the association of silver with the probe. In comparison it can be noted that the intensity of spectral lines of sulphur at 2.3 keV and oxygen at 0.5 keV has a speculative decrease from that of the free probe **CR-3**, and this may be affirmed that the thiocarbonyl sulphur atom and the hydroxyl oxygen atom have involved in oordination with Ag^+ ion. Hence, from the EDX analysis of the probe and the complex a consistent result was attained in agreement with the formerly illustrated analytical evidences.

Cytotoxicity and Cell Imaging

The MTT assay was adopted to reveal the cytotoxicity of the probe **CR-3** on HeLa cells through determination of cell validation at varying dose of **CR-3** incubated and as time dependent assay. The dose dependent cytotoxic assay was done with different dose of **CR-3** in HeLa cell lines for 1 h of incubation period as shown in Fig. S11, where it was noticed that to the extent of 20 μM dose of **CR-3** probe, only very small percentage of cells were degraded, this shows the non-cytotoxic nature of the probe to a admissible concentration level. Also, the cell viability assay of HeLa cell lines incubated with 10 μM **CR-3** at various time lapses as presented in Fig. S12, which demonstrates that to a time course of 24 h the cell viability rate is quite stable and only a small percentage loss of cell lines were noted. Also, the half maximal inhibitory concentration value of **CR-3** (Ic_{50}) in HeLa cell lines for 48 h of incubation at concentration of 1 μM, 10 μM, 50 μM, 100 μM, and 250 μM (1% DMSO, 99% serum free EMEM), was performed and Ic_{50} value was determined to be 49.69 μmol).

Hence, the MTT assay illustrates that the probe **CR-3** doesn't produce any adverse effect on cell viability.

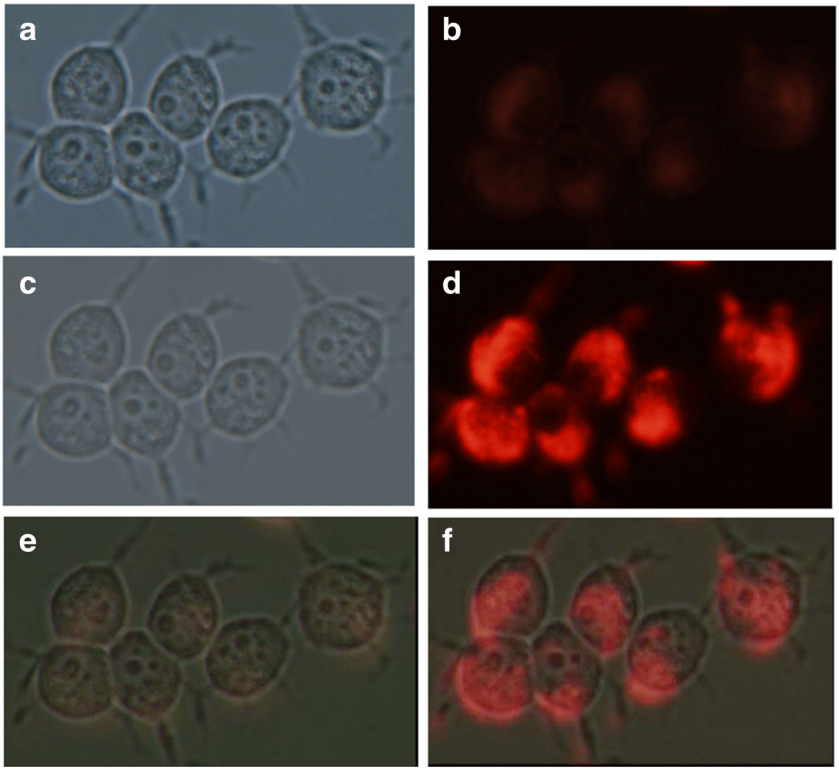

Fig. 12 Live imaging of Ag (I) ions in HeLa cells by **CR-3**. **a** Bright field image of HeLa cells incubated with **CR-3**. (10 μM) for 30 min at 37 °C. **b** Fluorescence image of HeLa cells incubated with **CR-3** (10 μM). **c** Bright field images of **CR-3** (10 μM) treated HeLa cells with Ag^+ (10 μM). **d** Fluorescence image of **CR-3** (10 μM) treated HeLa cells with Ag^+ (10 μM). **e** Overlay image of (a) and (b). **f** Overlay image of (c) and (d)

Thus, an optimal concentration of 10 μM of **CR-3** with an incubation period below 1 h was followed in all the confocal imaging studies.

The fluorescence surface imaging of HeLa cell lines was performed for detection of Ag^+ ion in HeLa cells by intrusion of **CR-3** probe in the cell line. About 10 μM of **CR-3** in phosphate buffered saline (pH 7.5) and DMSO/H_2O (1:9) with EMEM was incubated in the cell lines for period of 30 min, and after washing with buffer solution the cells were monitored with confocal microscope. The surface morphograph of probe **CR-3** alone incubated cell lines shown in Fig. 12a, b depicts the bright field images with clear cell morphology and in the florescence field images were blurred and darken.

However, when the cells lines were further incubated with 10 μM Ag^+ ions in aqueous solution, the cell lines were dull in the Bright field, whilst in the fluorescent light the HeLa cell micrographs were labelled in fluorescent red (Fig. 12c, d), this shows the **CR-3** + Ag^+ complex formation in the cell lines. Also, the overlay images (Fig. 12e & d) clearly show the distinguishable fluorescent detection of Ag^+ ions in cells. These observations demonstrates that the probe **CR-3** were cell permeable and can be efficiently used for in-vitro imaging of Ag^+ ions in living cells. Moreover, there were least indications of cell damages, cells were intact and showed adherent morphology during and after the labelling process with probe **CR-3**, indicating the least cytotoxic effects.

Conclusions

The developed carbazole – rhodanine sensor (**CR-3**) is highly selective, sensitive towards silver ion through strong intramolecular charge transfer from carbazole (donor) to rhodanine-3-acetic acid (receptor) with a lowest detection limit of 12.8×10^{-9} M and high quantum efficiency. The fluorescent probe-metal (**CR-3** + Ag^+) complex was reversible with 1 equivalent of I^- ion that ascertained the reutilization of probe with minimal efficiency loss. Also the influencing magnitude of factors such that the interfering metal ion, fluorescence standing time, and temperature effect on the optical detection of Ag^+ ion of **CR-3** was appreciable and less indeed. In compliment, the carbazole – rhodanine based sensor was proven to be biocompatible, non-cytotoxic and capable of fluorescence detection of Ag^+ ion in live cells.

Acknowledgements C. Denzil Britto is thankful to DST-SERB, New Delhi, India, for project fellowship and K. Sekar is grateful to DST-SERB, New Delhi, India, for financial support. (Grant No: SB/FT/CS-062/2013)

References

1. Drake PL, Hazelwood KJ (2005) Exposure-related health effects of silver and silver compounds: a review. Ann Occup Hyg 49(7):575–585

2. Modak SM, Sampath L, Fox CL Jr (1988) Combined topical use of silver sulfadiazine and antibiotics as a possible solution to bacterial resistance in burn wounds. J Burn Care Rehabil 9:359–363
3. Gulbranson SH, Hud JA, Hansen RC (2000) Argyria following the use of dietary supplements containing colloidal silver protein. Cutis 66:373–374
4. Monteiro DR, Gorup LF, Takamiya AS, Ruvollo-Filho AC, de Camargo ER, Barbosa DB (2009) The growing importance of materials that prevent microbial adhesion: antimicrobial effect of medical devices containing silver. Int J Antimicrob Agents 34:103–110
5. Hogstrand C, Wood CM (1998) Toward a better understanding of the bioavailability, physiology, and toxicity of silver in fish: implications for water quality criteria. Environ Toxicol Chem 17(4):547–561
6. Yu C, Zhang J, Ding M, Chen L (2012) Silver(I) ion detection in aqueous media based on "off-on" fluorescent probe. Anal Methods 4:342–344
7. Liu L, Zhang G, Xiang J, Zhang D, Zhu D (2008) Fluorescence "turn on" Chemosensors for Ag^+ and Hg^{2+} based on Tetraphenylethylene motif featuring adenine and thymine moieties. Org Lett 10(20):4581–4584
8. Huang C, Ren A, Feng C, Yang N (2010) Two-photon fluorescent probe for silver ion derived from twin-cyano-stilbene with large two-photon absorption cross section. Sensors Actuators B Chem 151:236–242
9. Zhang B, Sun J, Bi C, Yin G, Pu L, Shi Y, Sheng L (2011) A highly selective ratiometric fluorescent chemosensor for Ag^+ based on a rhodanineacetic acid-pyrene derivative. New J Chem 35:849–853
10. Yan H, Su H, Tian D, Miao F, Li H (2011) Synthesis of triazolothiadiazole fluorescent organic nanoparticles as primary sensor toward Ag^+ and the complex of Ag^+ as secondary sensor toward cysteine. Sensors Actuators B Chem 160:656–661
11. Ye J-H, Duan L, Yan C, Zhang W, He W (2012) A new ratiometric Ag^+ fluorescent sensor based on aggregation-induced emission. Tetrahedron Lett 53:593–596
12. Zhang X-B, Hana Z-X, Fang Z-H, Shen G-L, Ru-Qin Y (2006) 5, 10,15-Tris(pentafluorophenyl)corrole as highly selective neutral carrier for a silver ion-sensitive electrode. Anal Chim Acta 562: 210–215
13. Mahajan RK, Soon P, Mahajan MP, Singh P (2004) 2,6-Bis-methylsulfanyl-[1,3,5]thiadiazine-4-thione as a Ag^+-selective Ionophore. Anal Sci 20:1423–1426
14. Foldbjerg R, Dang DA, Autrup H (2011) Cytotoxicity and genotoxicity of silver nanoparticles in the human lung cancer cell line, A549. Arch Toxicol 85:743–750
15. Kaegi R, Sinnet B, Zuleeg S, Hagendorfer H, Mueller E, Vonbank R, Boller M, Burkhardt M (2010) Release of silver nanoparticles from outdoor facades, Environmental Pollution. Environ Pollut 158:2900–2905
16. Ahamed M, Al Salhi MS, Siddiqui MKJ (2010) Silver nanoparticle applications and human health. Clin Chim Acta 411:1841–1848
17. Di Vincenzo GD, Giordano CJ, Schriever LS (1985) Biologic monitoring of workers exposed to silver. Int Arch Occup Environ Health 56:207–215
18. Drake PL, Marcy AD, Ashley K (2006) Evaluation of a standardized method for determining soluble silver in workplace air samples. J Environ Monit 8:134–139
19. Velmurugan K, Raman A, Easwaramoorthi S, Nandhakumar R (2014) Pyrene pyridine-conjugate as Ag selective fluorescent chemosensor. RSC Adv 4:35284–35289
20. Kandaz M, Guney O, Senkal FB (2009) Fluorescent chemosensor for Ag(I) based on amplified fluorescence quenching of a new phthalocyanine bearing derivative of benzofuran. Polyhedron 28: 3110–3114
21. Zheng H, Yan M, Fan X-X, Sun D, Yang S-Y, Yang L-J, Li J-D, Jiang Y-B (2012) A heptamethine cyanine-based colorimetric and ratiometric fluorescent chemosensor for the selective detection of Ag^+ in an aqueous medium. Chem Commun 48:2243–2245
22. Wang H-H, Xue L, Qian Y-Y, Jiang H (2010) Novel Ratiometric fluorescent sensor for silver ions. Org Lett 12(2):292–295
23. Wang F, Nandhakumar R, Moon JH, Kim KM, Lee JY, Yoon J (2011) Ratiometric fluorescent Chemosensor for silver ion at physiological pH. Inorg Chem 50:2240–2245
24. Li C-Y, Xu F, Li Y-F (2010) A fluorescent chemosensor for silver ions based on porphyrin compound with high selectivity. Spectrochim Acta A 76:197–201
25. Asiri AM, Osman OI, Al-Thaqafy SH, Khan SA (2017) Optical properties and fluorescence quenching of carbazole containing (D–π–a) push–pull chromophores by silver nanoparticles: a detailed insight *via* an experimental and theoretical approach. RSC Adv 7:8402–8414
26. Dang F, Lei K, Liu W (2008) A new highly selective fluorescent silver probe. J Fluoresc 18:149–153
27. Zhang JF, Zhou Y, Yoon J, Kim JS (2011) Recent progress in fluorescent and colorimetric chemosensors for detection of precious metal ions (silver, gold and platinum ions). Chem Soc Rev 40: 3416–3429
28. Khatua S, Schmittel M (2013) A single molecular light-up sensor for quantification of Hg^{2+} and Ag^+ in aqueous medium: high selectivity toward Hg^{2+} over Ag^+ in a mixture. Org Lett 15(17):4422–4425
29. Hatai J, Pal S, Bandyopadhyay S (2012) Fluorescent detection of silver ions in water with organic nano-aggregates. RSC Adv 2: 10941–10947
30. Iyoshi S, Taki M, Yamamoto Y (2008) Rosamine-based fluorescent Chemosensor for selective detection of silver(I) in an aqueous solution. Inorg Chem 47:3946–3948
31. Wang H, Xue L, Jiang H (2011) Ratiometric fluorescent sensor for silver ion and its resultant complex for iodide anion in aqueous solution. Org Lett 13(15):3844–3847
32. Jang S, Thirupathi P, Neupane LN, Seong J, Lee H, Lee WI, Lee K-H (2012) Highly sensitive ratiometric fluorescent chemosensor for silver ion and silver nanoparticles in aqueous solution. Org Lett 14(18):4744–4749
33. Liu C, Huang S, Yao H, He S, Lu Y, Zhao L, Zeng X (2014) Preparation of fluorescein-based chemosensors and their sensing behaviors toward silver ions. RSC Adv 4:16109–16114
34. Huang S, He S, Lu Y, Wei F, Zeng X, Zhao L (2011) Highly sensitive and selective fluorescent chemosensor for Ag^+ based on a coumarin–Se_2N chelating conjugate. Chem Commun 47:2408–2410
35. Shi D-T, Wei X-L, Sheng Y, Zang Y, He X-P, Xie J, Liu G, Tang Y, Li J, Chen G-R (2014) Substitution pattern reverses the fluorescence response of Coumarin Glycoligands upon coordination with silver (I). Sci Rep 4:4252
36. Liu L, Zhang D, Zhang G, Xiang J, Zhu D (2008) Highly selective Ratiometric fluorescence determination of Ag^+ based on a molecular motif with one pyrene and two adenine moieties. Org Lett 10(11):2271–2274
37. Jang S, Thirupathi P, Neupane LN, Seong J, Lee H, In Lee W, Lee K-H (2012) Highly sensitive Ratiometric fluorescent Chemosensor for silver ion and silver nanoparticles in aqueous solution. Org Lett 14(18):4746–4749
38. Yang R-H, Chan W-H, Lee AWM, Xia P-F, Zhang H-K, Li K'A (2003) A Ratiometric fluorescent sensor for Ag^I with high selectivity and sensitivity. J Am Chem Soc 125:2884–2885
39. Chatterjee A, Santra M, Won N, Kim S, Kim JK, Kim SB, Ahn KH (2009) Selective Fluorogenic and chromogenic probe for detection of silver ions and silver nanoparticles in aqueous media. J Am Chem Soc 131:2040–2041
40. Li C-Y, Kong X-F, Li Y-F, Zou C-X, Liu D, Zhu W-G (2013) Ratiometric and colorimetric fluorescent chemosensor for Ag^+ based on tricarbocyanine. Dyes Pigments 99:903–907

41. Wu TY, Tsao MH, Chen FL, Su SG, Chang CW, Wang HP, Lin YC, Sun IW (2010) Synthesis and characterization of three organic dyes with various donors and Rhodanine ring acceptor for use in dye-sensitized solar cells. J Iran Chem Soc 7(3):707–720
42. Sk B, Khodia S, Patra A (2018) T and V-shaped donor–acceptor–donor molecules involving pyridoquinoxaline: large stokes shift, environment-sensitive tunable emission and temperature-induced fluorochromism. Chem Commun 54:1786–1789
43. Balsukuri N, Guptam I (2017) Singlet-singlet energy transfer in carbazole-porphyrin dyads and triads. Dyes Pigments 144:223–233
44. Dumat B, Bordeau G, Aranda AI, Mahuteau-Betzer F, El Harfouch Y, Metgé G, Charra F, Fiorini-Debuisschert C, Teulade-Fichou M-P (2012) Vinyl-triphenylamine dyes, a new family of switchable fluorescent probes for targeted two-photon cellular imaging: from DNA to protein labelling. Org Biomol Chem 10:6054–6061
45. Gong W-L, Zhong F, Aldred MP, Fu Q, Chen T, Huang D-K, Shen Y, Qiao X-F, Ma D, Zhu M-Q (2012) Carbazole oligomers revisited: new additions at the carbazole 1- and 8-positions. RSC Adv 2:10821–10828
46. Mingming H, Liu Y, Yi C, Song W, Gao L, Haichuan M, Huangd J, Jianhua S (2017) Highly efficient triazine/carbazole-based host material for green phosphorescent organic light-emitting diodes with low efficiency roll-off. RSC Adv 7:7287–7292
47. Stoeck U, Senkovska I, Bon V, Krause S, Kaskel S (2015) Assembly of metal–organic polyhedra into highly porous frameworks for ethene delivery. Chem Commun 51:1046–1049
48. Głuszyñska A (2015) Biological potential of carbazole derivative. Eur J Med Chem 94:405–426
49. Denzil Britto C, Muthu Vengaian K, Sekar K, Sivaraman G, Singaravadivel S (2017) Carbazole-azine based fluorescence 'off–on' sensor for selective detection of Cu^{2+} and its live cell imaging. Luminescence 32(7):1354–1360
50. Fan L, Gao S-Q, Li Z-B, Niu W-F, Zhang W-J, Shuang S-M, Dong C (2015) An indole-carbazole-based ratiometric emission pH fluorescent probe for imaging extreme acidity. Sensors Actuators B Chem 221:1069–1076
51. Feng Y, Li D, Wang Q, Wang S, Meng X, Shao Z, Zhu M, Wang X (2016) A carbazole-based mitochondria-targeted two-photon fluorescent probe for gold ions and its application in living cell imaging. Sensors Actuators B Chem 225:572–578
52. Goswami S, Paul S, Manna A (2013) Carbazole based hemicyanine dye for both "naked eye" and 'NIR' fluorescence detection of CN^- in aqueous solution: from molecules to low cost devices (TLC plate sticks). Dalton Trans 42:10682–10686
53. Kala K, Manoj N (2016) A carbazole based "turn on" fluorescent sensor for selective detection of Hg^{2+} in an aqueous medium. RSC Adv 6:22615–22619
54. Kaur M, Ahn Y-H, Choi K, Cho MJ, Choi DH (2015) A bifunctional colorimetric fluorescent probe for Hg^{2+} and Cu^{2+} based on a carbazole–pyrimidine conjugate: chromogenic and fluorogenic recognition on TLC, silica-gel and filter paper. Org Biomol Chem 13: 7149–7153
55. Li D, Sun X, Huang J, Wang Q, Feng Y, Chen M, Meng X, Zhu M, Wang X (2016) A carbazole-based "turn-on" two-photon fluorescent probe for biological Cu^{2+} detection *vis* Cu^{2+}-promoted hydrolysis. Dyes Pigments 125:185–191
56. Sharma S, Pradeep CP, Dhir A (2015) Dansyl-carbazole AIEE material for selective recognition of thiourea derivatives. New J Chem 39:1822–1826
57. Xu Q-c, Wang X-f, Xing G-w, Zhang Y (2013) Carbazole substituted 2-aminobenzamide compounds: synthesis, fluorescence ON–OFF–ON sensing of Zn(II) and PPi ions, assay for alkaline phosphatase, and computational study. RSC Adv 3:15834–15841
58. Zhang J, Zhang L, Wei Y, Chao J, Wang S, Shuang S, Cai Z, Dong C (2013) A selective carbazole-based fluorescent probe for chromium(III). Anal Methods 5:5549–5554
59. El-Zawawy FM, El-Shahat MF, Mohamed AA, Zaki MTM (1995) Spectrophotometric determination of silver and gold with 5-(2,4-dihydroxybenzylidene)rhodanine and cationic surfactants. Analyst 120:549–554
60. Godoy RE, Perez AG (1986) Spectrophotometric determination of trace amounts of silver with 5-[4-(2-methyl-3-hydroxy-5-hydroxymethyl)pyridylene]rhodanine. Analyst 111:1297–1299
61. Borissova R, Koeva M, Topalova E (1975) Prediction of conditions for use of spectrophotometric reagents: p-dimethyl amino benzilidene rhodanine as a spectrophotometric reagent for silver and palladium. Talanta 22:791–796
62. Song J, Kong H, Jang J (2011) Adsorption of heavy metal ions from aqueous solution by polyrhodanine-encapsulated magnetic nanoparticles. J Colloid Interface Sci 359:505–511
63. Jabeen S, Dines TJ, Withnall R, Leharne SA, Chowdhry BZ (2009) Surface-enhanced Raman scattering studies of rhodanines: evidence for substrate surface-induced dimerization. Phys Chem Chem Phys 11:7476–7483
64. Moers FG, Steggerda JJ (1968) Copper complexes of rhodanine and its 3-alkyl derivatives. J Inorg Nucl Chem 30:3217–3222
65. Sandell EB, Neumayer JJ (1951) Photometric determination of traces of silver. Anal Chem 23(12):1863–1865
66. Ostrauskaite J, Voska V, Antulis J, Gaidelis V, Jankauskas V, Grazulevicius JV (2002) High hole mobilities in carbazole-based glass-forming hydrazones. J Mater Chem 12:3469–3474
67. Meyer T, Ogermann D, Pankrath A, Kleinermanns K, Muller TJJ (2012) Phenothiazinyl Rhodanylidene Merocyanines for dye-sensitized solar cells. J Org Chem 77:3704–3715
68. Conners KA (1987) Binding constants - the measurement of molecular complex stability. John Wiley & Sons, New York
69. Shortreed M, Kopelman R, Kuhn M, Hoyland B (1996) Fluorescent fiber-optic calcium sensor for physiological measurements. Anal Chem 68:1414–1418
70. Helm DV, Lessor AE, Merritt LLJ (1962) The crystal structure of rhodanine $C_3H_3ONS_2$. Acta Cryst 15:1227–1232
71. Marzec KM, Gawel B, Lasocha W, Proniewicz LM, Malek K (2010) Interaction between rhodanine and silver species on a nanocolloidal surface and in the solid state. J Raman Spectrosc 41:543–552
72. Stephen WI, Townshend A (1965) The reaction of silver(I) ions with organic reagents containing the HN-C=S grouping. Part I. Rhodanine and related compounds. J Chem Soc 0:3738–3746
73. Tejchman W, Skorska-Stania A, Zesławska E (2016) The Crystal Structures of Three Rhodanine-3-Carboxylic Acids. J Chem Crystallogr 46(4):181–187
74. Walker LA, Folting K, Merritt LL (1969) The crystal structure of 2-thiohydantoin, $C_3H_4ON_2S$. Acta Cryst B25:88–93
75. Risch MJ, Trucks GW, Schlegel HB, Scuseria GE, Robb MA, Cheeseman JR, Scalmani G, Barone V, Mennucci B, Petersson GA, Nakatsuji H, Caricato M, Li X, Hratchian HP, Izmaylov AF, Bloino J, Zheng G, Sonnenberg JL, Hada M, Ehara M, Toyota K, Fukuda R, Hasegawa J, Ishida M, Nakajima T, Honda Y, Kitao O, Nakai H, Vreven T, Montgomery JA Jr, Peralta JE, Ogliaro F, Bearpark M, Heyd JJ, Brothers E, Kudin KN, Staroverov VN, Kobayashi R, Normand J, Raghavachari K, Rendell A, Burant JC, Iyengar SS, Tomasi J, Cossi M, Rega N, Millam JM, Klene M, Knox JE, Cross JB, Bakken V, Adamo C, Jaramillo J, Gomperts R, Stratmann RE, Yazyev O, Austin AJ, Cammi R, Pomelli C, Ochterski JW, Martin RL, Morokuma K, Zakrzewski VG, Voth GA, Salvador P, Dannenberg JJ, Dapprich S, Daniels AD, Farkas O, Foresman JB, Ortiz JV, Cioslowski J, Fox DJ (2009) Gaussian 09, Revision A.02. Gaussian, Inc., Wallingford
76. Velmurugan K, Thamilselvan A, Antony R, Kannan VR, Tang L, Nandha kumar R (2017) Imidazoloquinoline bearing thiol probe as fluorescent electrochemical sensing of ag and relay recognition of proline. J Photochem Photobiol A Chem 333:130–141